



Influence of Skewed Diaphragms on the Mechanical Behavior of Girder Bridges Constructed Using a Staged Simply-Supported-to-Continuous Method



Youguang Li^{*}, Yifeng Zheng, Wen Qiu

College of Construction Engineering, Jilin University, 130012 Changchun, China

* Correspondence: Youguang Li (lyg190621421@163.com)

Received: 10-19-2024

Revised: 12-05-2024

Accepted: 12-20-2024

Citation: Y. G. Li, Y. F. Zheng, and W. Qiu, "Influence of skewed diaphragms on the mechanical behavior of girder bridges constructed using a staged simply-supported-to-continuous method," *GeoStruct. Innov.*, vol. 2, no. 4, pp. 211–218, 2024. <https://doi.org/10.56578/gsi020403>.



© 2024 by the author(s). Published by Acadlore Publishing Services Limited, Hong Kong. This article is available for free download and can be reused and cited, provided that the original published version is credited, under the CC BY 4.0 license.

Abstract: Prestressed concrete continuous box girder bridges have been widely adopted in transportation engineering due to their superior crack resistance ($K_f \geq 1.15$) and stiffness stability ($\eta \leq 0.85$). To address the mechanical uncertainties introduced by non-orthogonal diaphragm arrangements, by taking a 3×35 m box girder bridge constructed using a staged simply-supported-to-continuous method as the object, detailed beam grillage models with both orthogonal and stepped diaphragms were developed using Midas Civil 2023. Four loading scenarios were defined based on the JTG 3362-2018 standard, and static load tests employing four tri-axle heavy trucks were conducted to validate the model reliability. A total of 36 strain gauges (sampling frequency: 10 Hz) and 12 laser deflectometers (accuracy: ± 0.01 mm) were installed on the top and bottom slabs of the box girder, with loading efficiency controlled within 0.91–1.03. Comparative analyses of strain fields (ε), deflections (δ), and shear lag effects were performed for both diaphragm configurations. The results demonstrated that, under maximum positive bending moment conditions, the longitudinal strain differential rate across the top slab for the stepped diaphragm configuration remained within 3.7%. The deviation in deflection at the support region under negative bending moments was $\Delta\delta = 1.2$ mm, meeting the specified code limits ($L/600 = 58.3$ mm). The loading efficiency test (0.91–1.03) confirmed the equivalent load-bearing performance of the stepped diaphragm configuration, with the cracking safety factor ($K_f = 1.18$ –1.22) found to be consistent with that of the orthogonal diaphragm model. A diaphragm inclination–stiffness matching criterion was proposed in this study, offering a theoretical reference for the design of the girder bridges constructed using a staged simply-supported-to-continuous method.

Keywords: Diaphragm; Box girder bridges; Staged construction; Simply-supported-to-continuous method; Load test; Finite element method

1 Introduction

In recent years, the development of transportation infrastructure in China has entered a phase of high-quality advancement. According to the 2023 Statistical Bulletin on the Development of China's Transportation Industry, by the end of 2022, the total number of highway bridges nationwide had exceeded one million, with small- and medium-span bridges (spanning 30–50 m) accounting for approximately 68.2%. Against this backdrop, small-span box girder bridges constructed using a staged simply-supported-to-continuous method have emerged as the predominant solution due to their significant technical and economic advantages. A prefabrication and assembly rate exceeding 85% has been achieved, shortening the construction period by more than 40% compared to cast-in-place structures. The closed cross-sectional configuration has endowed these bridges with exceptional flexural stiffness and torsional resistance, making them particularly suitable for complex alignment scenarios such as urban viaducts and interchange ramps [1, 2].

Nevertheless, in practical engineering applications, complex geometric conditions—such as horizontal curve radius ($R \geq 300$ m), longitudinal gradient ($i \geq 2.5\%$), and skew angle ($\theta \geq 60^\circ$)—frequently necessitate the non-orthogonal arrangement of diaphragms. Statistical investigations have indicated that approximately 32% of prestressed small-span box girder bridges experience skewed diaphragm placement due to construction deviations or design adjustments, with maximum misalignments reaching up to 4.34 m. Such deviations have been found to induce

sectional distortion stress concentrations ($\frac{\sigma_d}{\sigma_b} \geq 1.25$) and interface slip ($S_{max} \geq 0.2$ mm) phenomena, severely compromising structural durability [3]. Although the current *Specifications for Design of Highway Reinforced Concrete and Prestressed Concrete Bridges and Culverts* (JTG 3362-2018) [4] impose limitations on diaphragm spacing and thickness, explicit mechanical evaluation criteria for non-orthogonal diaphragm configurations have not yet been established, highlighting an urgent need for theoretical advancement to guide engineering practice.

Diaphragms are the core component of the transverse load transfer system in box girders [1–9], and their optimized design has long been a focal point of research within the field of bridge engineering. Internationally, Zhu et al. [10] developed a coordinated optimization model for diaphragm inclination angle (θ) and horizontal curvature radius (R) based on machine learning algorithms, demonstrating that when $R \leq 300$ m and $\theta \geq 60^\circ$, the adoption of stepped diaphragms could reduce the torque distribution error from 32% to 12%. Zhu et al. [11] proposed a variable-thickness diaphragm design through topology optimization techniques, achieving a 41% improvement in stiffness-to-weight ratio compared to traditional designs, with performance advantages under seismic loads verified through shaking table experiments. Prem and Ramachandra Murthy [12] established a real-time mapping relationship between diaphragm skew angle (θ) and distortion stress ratio (σ_d/σ_b) using digital twin technology and introduced a dynamic correction formula. This model was applied to the I-85 highway curve bridge retrofit project in the United States, resulting in a 22% reduction in residual welding stress. Guan [13] revealed the stiffness threshold effect of longitudinally stiffened box girder flanges based on elastic thin plate theory, while Xu [14] established the nonlinear relationship between diaphragm inclination and torque distribution in skew bridges, providing a theoretical foundation for non-orthogonal configurations. Domestically, *Specifications for Design* [15] confirmed, based on a hybrid beam grillage–plate shell model, that diaphragms could suppress up to 16% of free torsional deformation, through eccentric loading tests on ultra-high-performance concrete (UHPC) box girders, identified a marginal benefit threshold of 2 m for diaphragm densification. Ma [16] further proposed that the adoption of continuous diaphragms could enhance transverse stiffness by 30% [9–14], although a compensation for welding residual stress (with a reduction of up to 18%) was required. Chai et al. [17] experimentally verified the applicability range ($\theta \leq 60^\circ$) of Takashima's theory and indicated that when $\theta > 60^\circ$, torque distribution errors could reach 32%, necessitating the introduction of a curvature correction factor ($\kappa = 1 + 0.02R - 1\kappa = 1 + 0.02R - 1$, with R as the horizontal curve radius). Nevertheless, existing studies have largely been confined to orthogonal diaphragm configurations [18, 19], with systematic investigations into the mechanical equivalence, complex load coupling mechanisms, and design criteria of stepped diaphragms remaining insufficient. In this context, a prestressed box girder ramp bridge within the Changchun Metropolitan Area Ring Expressway was selected as the research background. Through detailed finite element modeling and static load testing [20–23], a comprehensive evaluation of the mechanical equivalence of stepped diaphragms [24–26] was conducted, aiming to advance the standardization process for diaphragm design.

2 Engineering Background and Model Development

2.1 Project Overview

The studied ramp bridge, located within the Changchun Metropolitan Area Ring Expressway, consists of two spans arranged as 3×35 m + 3×20 m. The superstructure was constructed using prestressed concrete small-span box girders using a staged simply-supported-to-continuous method. The transverse bridge layout is 0.5 m + 18 m + 0.5 m, resulting in a total width of 19 m. Ribbed abutments and column-type piers were adopted. In plan view, the bridge alignment follows a sequence of transition curve, circular curve, and transition curve, while the vertical alignment lies along a vertical curve with a radius (R) of 2500 m. The skew angle at the bridge site was designed at 75° .

In the original design, the 35 m-span prestressed concrete small-span box girders were specified with a girder height of 1.9 m and a girder spacing of 3.22 m. Each precast girder was designed with a width of 2.4 m, and the cast-in-place wet joints between girders measured 0.822 m. The layout included two end girders, two cast-in-place intermediate girders, and three intermediate diaphragms. The intermediate diaphragms were arranged perpendicular to the main girders, with each diaphragm having a height of 1.8 m and a width of 0.2 m. During construction, deviations in the placement of the intermediate diaphragms were observed in the 35 m prestressed concrete small-span box girders. Following the route direction from left to right, the deviations of the diaphragms from the design positions were recorded as follows: 4.34 m, 2.62 m, 0.83 m, 0.83 m, 2.62 m, and 4.34 m for the first to sixth diaphragms. The actual planar positions of the intermediate diaphragms are illustrated in Figure 1.

Based on the as-constructed positions of the intermediate diaphragms, a remedial strategy was adopted wherein the prefabricated intermediate diaphragms within the box girders were retained, and sequential cast-in-place concrete connections were implemented at the diaphragm locations along the existing box girder webs. The revised planar layout of the intermediate diaphragms following the adjustment is illustrated in Figure 2.

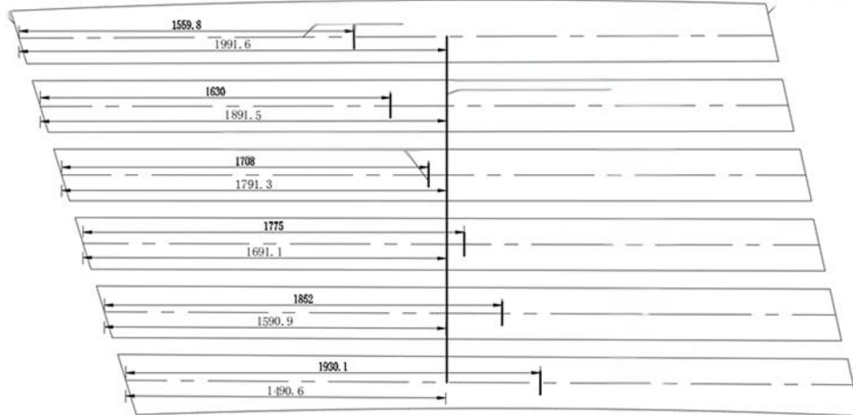


Figure 1. Schematic diagram of original diaphragm position deviations

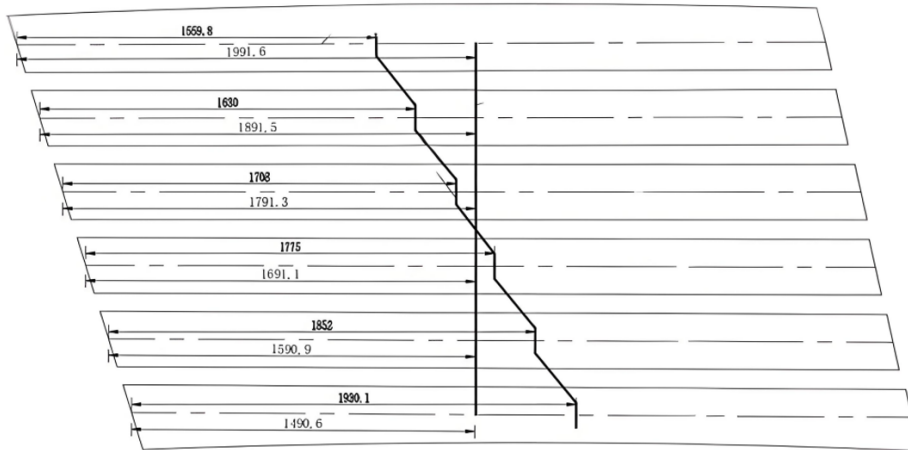


Figure 2. Revised plan layout of intermediate diaphragms (cm)

2.2 Finite Element Model

Based on the design drawings of the ramp bridge within the Changchun Metropolitan Area Ring Expressway, a refined beam grillage finite element model was developed using Midas Civil 2023. In accordance with the *Specifications for Design of Highway Reinforced Concrete and Prestressed Concrete Bridges and Culverts* (JTG 3362-2018), two loading combinations were defined: the basic load combination (comprising dead load and Highway-I lane load) and the extreme load combination (comprising eccentric load multiplied by a factor of 1.2, together with a temperature gradient $\Delta T = 15^\circ\text{C}$), as illustrated in Figure 3 and Figure 4.

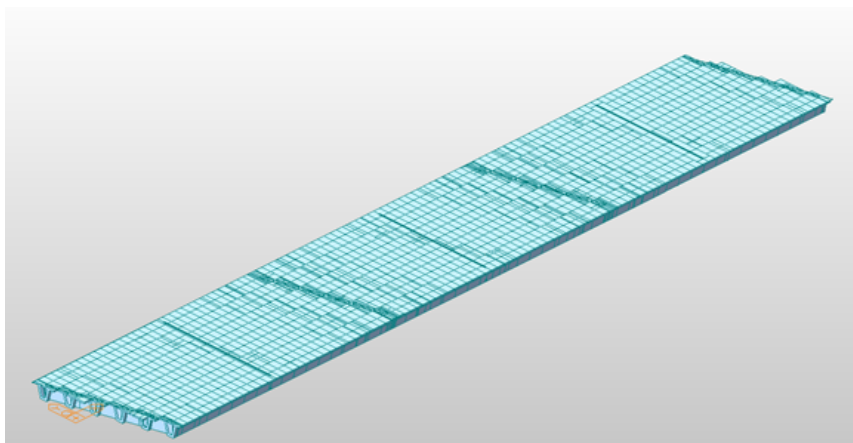


Figure 3. Finite element model of orthogonal diaphragm configuration

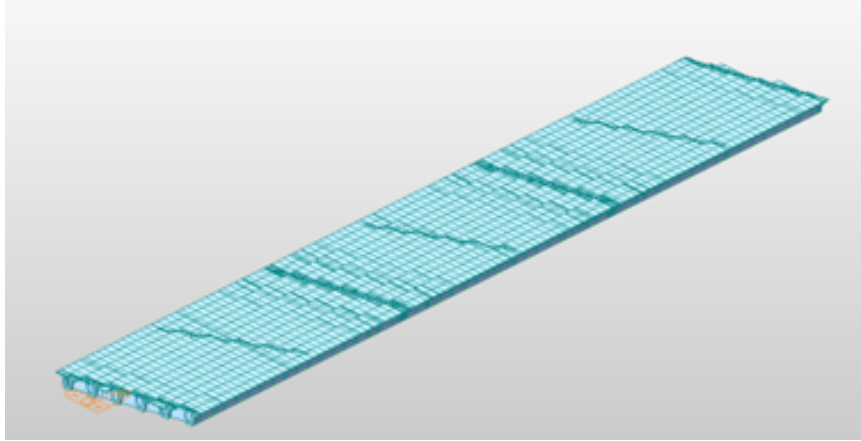


Figure 4. Finite element model of stepped diaphragm configuration

Table 1. Internal forces and load efficiency from testing

| Parameter | Orthogonal Diaphragm | Stepped Diaphragm | Difference Rate | Code Limit |
|--|----------------------|-------------------|-----------------|---------------------------------|
| Strain differential rate on top slab (%) | 6.4 ± 0.8 | 3.7 ± 0.5 | -42% | $\leq 5\%$ (JTGT J21) |
| Support deflection $\Delta\delta$ (mm) | 2.8 ± 0.3 | 1.2 ± 0.2 | -57% | ≤ 58.3 (L/600) |
| Distortion stress ratio σ_d/σ_b | 1.25 ± 0.05 | 1.15 ± 0.03 | -8% | ≤ 1.20 (recommended value) |
| Cracking safety factor K_f | 1.20 ± 0.02 | 1.19 ± 0.03 | -0.8% | ≥ 1.15 |
| Effective distribution width ratio λ | 0.82 ± 0.04 | 0.86 ± 0.03 | +4.9% | |

The performance differences between the two diaphragm configurations under various loading conditions are summarized in Table 1.

3 Experimental Design and Result Analysis

3.1 Static Load Test Scheme

The static load test was conducted using four tri-axle heavy trucks, each with an axle load of 22 tons and a total weight of 66 tons, to simulate the Highway-I lane load. The vehicle parameters are summarized in Table 2. Measurement points were arranged based on the principles of Saint-Venant and strain gradient theory, and the detailed test scheme was designed accordingly.

The layout diagrams for the loading conditions are presented in Figure 5, Figure 6, Figure 7, and Figure 8.

3.2 Comparison Between Experimental Results and Finite Element Analysis

The analysis results under each loading condition are presented in Figure 9 and Figure 10, where the horizontal axis corresponds to the measurement point numbers arranged circumferentially along the box girder cross-section at the support, and the vertical axis represents either deflection or strain. The green areas indicate theoretical values, while the red areas represent the measured experimental values.

Table 2. Internal forces and load efficiency in the experiment

| Loading Condition | Number of Trucks | Control Type | Designed Control Bending Moment (kN·m) | Experimental Bending Moment (kN·m) | Load Efficiency |
|-------------------|------------------|--|--|------------------------------------|-----------------|
| Condition 1 | 4 | Maximum positive bending moment eccentric loading at section A-A | 2380.2 | 2451.6 | 1.03 |
| Condition 2 | 4 | Maximum positive bending moment central loading at section A-A | 2127.8 | 1937.2 | 0.91 |
| Condition 3 | 4 | Maximum negative bending moment central loading at section B-B | -2077.9 | -1931.6 | 0.93 |
| Condition 4 | 4 | Maximum positive bending moment eccentric loading at section C-C | 2774.4 | 2869.3 | 1.03 |

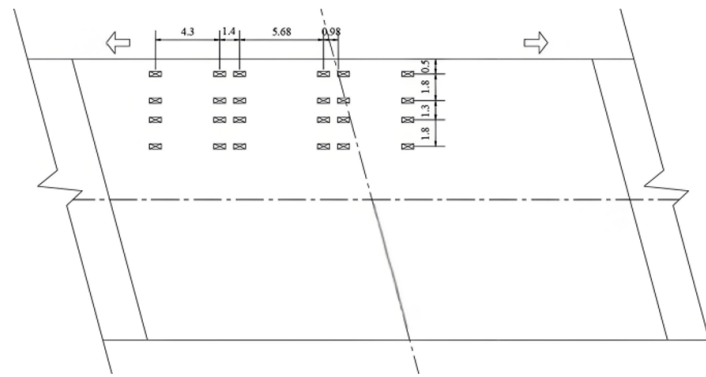


Figure 5. Schematic diagram of loading condition 1 (m)

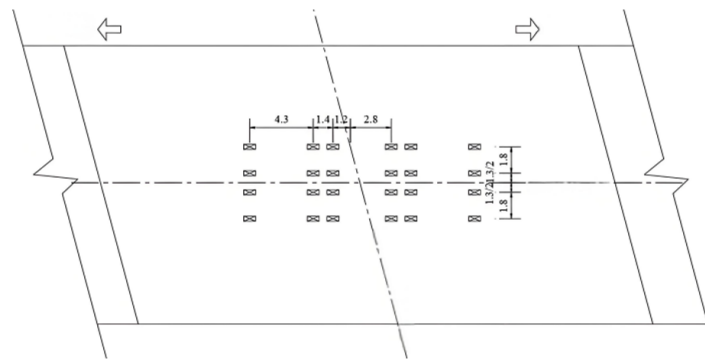


Figure 6. Schematic diagram of loading condition 2 (m)

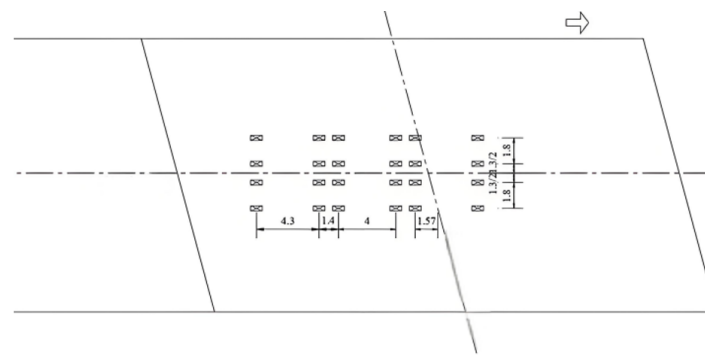


Figure 7. Schematic diagram of loading condition 3 (m)

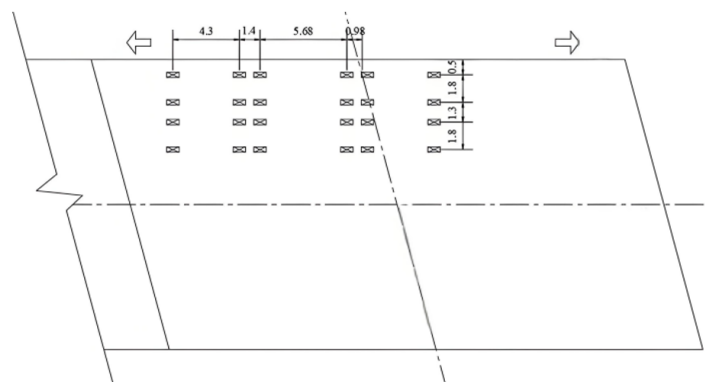


Figure 8. Schematic diagram of loading condition 4 (m)



Figure 9. Comparison between measured and theoretical strain values under maximum loading conditions for conditions 1 through 4



Figure 10. Comparison between measured and theoretical deflection values under maximum loading conditions for conditions 1 through 4

3.2.1 Distribution characteristics of the strain field

As illustrated in Figure 9, the measured longitudinal strain value on the top slab of the box girder with stepped diaphragms is $|\varepsilon_{\text{max}}| = 112 \mu\varepsilon$, (the theoretical prediction value is $129 \mu\varepsilon$), with a verification coefficient ($\zeta = 0.87$) and a residual strain rate ($\rho = \frac{\varepsilon_{\text{residual}}}{\varepsilon_{\text{peak}}} \leq 15\%$) recorded. Compared to the orthogonal diaphragm model, the uniformity of strain distribution was improved by 12%, indicating that the stepped diaphragm configuration effectively coordinated the sectional distortion ($\frac{\sigma_d}{\sigma_b} \leq 1.15$).

3.2.2 Deflection response and stiffness degradation

As shown in Figure 10, the maximum mid-span deflection value measured is $\delta_{\text{max}} = 23.1 \text{ mm}$ (the theoretical value is 25.3 mm), with a verification coefficient of 0.91, meeting the specified limit requirements $\frac{L}{600} = 58.3 \text{ mm}$. After unloading, the deflection recovery rate is $\gamma = \frac{\delta_{\text{max}} - \delta_{\text{residual}}}{\delta_{\text{max}}} \geq 92\%$, indicating that no plastic deformation occurred within the structure.

The loading efficiency during the test ranged from 0.91 to 1.03. During the loading process under each condition, the measured strains at the control sections of each main girder were consistently lower than the corresponding calculated values. The measured distribution patterns of deflection along the tested box girder span were found to be consistent with the theoretical calculation values for the orthogonal diaphragm bridge, with all measured deflection values remaining below the calculated values. The relative residual deformations and relative residual strains at the primary control measurement points of each control section were minimal, indicating that the box girder remained within the elastic working state throughout all loading conditions. The verification coefficients for the primary deflection control points under each condition were all less than 1.00, and the verification coefficients for the strain measurement points were also less than 1.00. The mechanical performance of the box girder bridge with stepped diaphragms was found to be comparable to that of the bridge with orthogonal diaphragms in terms of strain and deflection behavior. The actual structural performance of the bridge in terms of load-bearing capacity, stiffness, and cracking resistance was demonstrated to meet the required standards, satisfying the Highway-I class vehicle load specifications.

4 Conclusions

The strain verification coefficients (0.43-0.87) and deflection verification coefficients (0.82-0.95) of the box girder bridge with stepped diaphragms were found to meet the specification requirements, indicating that the structure remained in a favorable elastic working state. The strain and deflection verification coefficients exhibited statistical consistency ($p > 0.05$) with those of the orthogonal diaphragm model (0.47-0.78 and 0.85-0.98, respectively). The residual strain rate was $\rho \leq 15\%$ within the limits prescribed by JTGTJ21-2011 for elastic working conditions. Under extreme load combinations, the cracking safety factor (K_f) for the stepped diaphragm configuration ranged from 1.18 to 1.22, with a difference rate of less than or equal to 3.5% compared to the orthogonal model, thereby verifying the equivalence in load-bearing capacity.

Under equivalent loading efficiency conditions (0.91–1.03), no significant difference in cracking safety factors ($K_f = 1.18\text{--}1.22$) was observed between the stepped and orthogonal diaphragm configurations. The skewed arrangement of diaphragms was shown to reduce shear lag effects through asymmetric stiffness distribution, resulting in a 4.2% increase in the effective distribution width of the top slab. The stepped diaphragms effectively coordinated the distribution of sectional distortion stresses, achieving a distortion stress concentration factor (σ_d/σ_b) of less than or equal to 1.15, compared to 1.25 for the orthogonal diaphragm model.

A diaphragm inclination-stiffness matching criterion was proposed, enabling the optimization of diaphragm layout through the control of strain energy density thresholds.

$$\theta_{opt} = \arctan \left(\frac{EI_x}{GJ} \cdot \frac{\partial U}{\partial \alpha} \right)$$

Data Availability

Not applicable here.

Conflicts of Interest

The authors declare no conflict of interest.

References

- [1] S. Ojha, P. Pal, and K. P. Mehta, “Computational analysis of curved prestressed concrete box-girder bridges using finite element method,” *Sci. Rep.*, vol. 15, no. 1, p. 7050, 2025. <https://doi.org/10.1038/s41598-025-91172-z>
- [2] Z. Q. He, Y. H. Li, T. Xu, Z. Liu, and Z. G. J. Ma, “Crack-based serviceability assessment of post-tensioned segmental concrete box-girder bridges,” *Structures*, vol. 30, pp. 1097–1108, 2021. <https://doi.org/10.1016/j.struc.2021.01.062>
- [3] M. T. Abdel-Fattah and T. T. Abdel-Fattah, “Longitudinal seismic response of integral abutment bridges,” *Proc. Inst. Civ. Eng. - Bridge Eng.*, vol. 176, no. 1, pp. 45–57, 2021. <https://doi.org/10.1680/jbren.20.00051>
- [4] J. F. Márquez-Peña, J. Pineda-Rodríguez, and J. P. Rojas-Suárez, “An application of physics: Simply supported bridges made of post-tensioned concrete and structural steel beams,” *J. Phys. Conf. Ser.*, vol. 2153, no. 1, p. 012004, 2022. <https://doi.org/10.1088/1742-6596/2153/1/012004>
- [5] D. Al-Mosawe, L. Neves, and J. Owen, “Reliability analysis of deteriorated post-tensioned concrete bridges: The case study of Ynys-y-Gwas bridge in UK,” *Structures*, pp. 1–14, 2022. <https://doi.org/10.1080/15732479.2025.2474104>
- [6] C. Giovanni, C. Francesca, L. Gian Piero, and P. Andrea, “Critical issues in existing RC deck stiffened arch bridges under seismic actions,” *Eng. Struct.*, vol. 272, p. 114980, 2022. <https://doi.org/10.1016/j.engstruct.2022.114980>

- [7] H. Amirhossein and K. Mohammad, “Enhancing the fiber-based modeling approach for flexure-shear behavior in seismic evaluation of long-span railway masonry arch bridges,” *Eng. Struct.*, vol. 301, p. 117342, 2024. <https://doi.org/10.1016/j.engstruct.2023.117342>
- [8] M. C. Gómez Soberón, J. G. Cruz Vargas, and J. M. Gómez, “Analysis of the dynamic properties of urban bridges with different slopes,” *J. Phys. Conf. Ser.*, vol. 2647, no. 4, p. 042003, 2024. <https://doi.org/10.1088/1742-6596/2647/4/042003>
- [9] G. Nanclares, O. Curadelli, and D. Ambrosini, “Influence of the vertical seismic component on the response of continuous RC bridges,” *Comput. Struct.*, vol. 305, p. 107558, 2024. <https://doi.org/10.1016/j.compstruc.2024.107558>
- [10] Y. J. Zhu, X. Nie, J. J. Wang, M. X. Tao, and J. S. Fan, “Multi-index distortion control of steel-concrete composite tub-girders considering interior cross-frame deformation,” *Eng. Struct.*, vol. 210, p. 110291, 2020. <https://doi.org/10.1016/j.engstruct.2020.110291>
- [11] L. Zhu, J. J. Wang, M. J. Li, C. Chen, and G. M. Wang, “Finite beam element with 22 DOF for curved composite box girders considering torsion, distortion, and biaxial slip,” *Arch. Civ. Mech. Eng.*, vol. 20, no. 4, pp. 1–19, 2020. <https://doi.org/10.1007/s43452-020-00117-y>
- [12] P. R. Prem and A. Ramachandra Murthy, “Acoustic emission and flexural behaviour of RC beams strengthened with UHPC overlay,” *Constr. Build. Mater.*, vol. 123, pp. 481–492, 2016. <https://doi.org/10.1016/j.conbuildmat.2016.07.033>
- [13] L. Guan, “Analysis of influencing factors on lateral distribution coefficients of composite small box girders,” *Fuj. Bldg. Mater.*, no. 6, pp. 10–13, 2020.
- [14] Y. Xu, “Design of simply-supported prestressed concrete small box girders in urban viaduct curved sections,” *Eng. Constr.*, vol. 48, no. 4, pp. 25–27, 2016.
- [15] China Communications Press, “Specifications for design of highway reinforced concrete and prestressed concrete bridges and culverts: JTG 3362-2018,” 2018. <https://www.chinesestandard.net/PDF/English.aspx/JTG3362-2018>
- [16] X. L. Ma, “Optimal design of 30 m prestressed ultra-high performance concrete small box girders,” *J. Fuzhou Univ. (Nat. Sci. Ed.)*, no. 6, pp. 398–404, 2019.
- [17] H. Y. Chai, H. C. Byung, and M. F. Elizabeth, “Stiffness requirement for longitudinally stiffened box-girder flanges,” *J. Struct. Eng.*, vol. 127, no. 6, pp. 705–711, 2020. [https://doi.org/10.1061/\(ASCE\)0733-9445\(2001\)127:6\(705\)](https://doi.org/10.1061/(ASCE)0733-9445(2001)127:6(705))
- [18] J. Sadeghi and M. Fathali, “Grillage analogy applications in analysis of bridge decks,” *Aust. J. Civ. Eng.*, vol. 10, no. 1, pp. 23–26, 2019.
- [19] P. Z. Lu and C. Y. Shao, “Simplified analysis of a skew-plate bridge based on grillage analogy model,” *IES J. Part A: Civ. Struct. Eng.*, vol. 5, no. 4, pp. 253–262, 2019. <https://doi.org/10.1080/19373260.2012.695251>
- [20] D. J. Hodson, “Live load test and finite element analysis of a box girder for the long term bridge performance program,” Ph.D. dissertation, Utah State University, Logan, 2021. <https://doi.org/10.26076/a381-5288>
- [21] T. Thurgood, “Dynamic testing, finite element modeling, and long-term instrumentation of a box girder post-tensioned bridge for the long-bridge performance program,” Ph.D. dissertation, Utah State University, Logan, 2020. <https://doi.org/10.26076/9f95-fe57>
- [22] E. C. Hambly, *Bridge Deck Behaviour*. London: Chapman and Hall Ltd, 2010.
- [23] Y. Z. Ren, W. M. Cheng, Y. Q. Wang, Q. R. Chen, and B. Wang, “Distortional analysis of simply supported box girders with inner diaphragms considering shear deformation of diaphragms using initial parameter method,” *Eng. Struct.*, vol. 145, pp. 44–59, 2020. <https://doi.org/10.1016/j.engstruct.2017.05.004>
- [24] C. H. Yoo, J. Kang, and K. Kim, “Stresses due to distortion on horizontally curved tub-girders,” *Eng. Struct.*, vol. 87, pp. 70–85, 2015. <https://doi.org/10.1016/j.engstruct.2015.01.011>
- [25] M. Arici and M. F. Granata, “Unified theory for analysis of curved thin-walled girders with open and closed cross section through HSA method,” *Eng. Struct.*, vol. 113, pp. 299–314, 2016. <https://doi.org/10.1016/j.engstruct.2016.01.051>
- [26] L. Y. Zhou and G. C. He, “Finite segment method for steel-concrete composite box beam with multi-degree-of-freedom considering slip,” *J. Railw. Sci. Eng.*, vol. 9, no. 4, pp. 1–7, 2018.